IEEE Access
Multidisciplinary ⋮ Rapid Review ⋮ Open Access Journal

Received 10 August 2024, accepted 25 August 2024, date of publication 10 September 2024, date of current version 2 October 2024.

Digital Object Identifier 10.1109/ACCESS.2024.3457030

RESEARCH ARTICLE

Joint Synchronization and Channel Estimation for GFDM Systems

ABUBAKAR MAGAJI BELLO[1], WATCHARAPAN SUWANSANTISUK[2], (Senior Member, IEEE), IICKHO SONG[3], (Fellow, IEEE), AND TAKUICHI HIRANO[4], (Senior Member, IEEE)

[1]Department of Computer Engineering, Faculty of Engineering, King Mongkut's University of Technology Thonburi, Bangkok 10140, Thailand
[2]Department of Electronic and Telecommunication Engineering, Faculty of Engineering, King Mongkut's University of Technology Thonburi, Bangkok 10140, Thailand
[3]School of Electrical Engineering, College of Engineering, Korea Advanced Institute of Science and Technology, Daejeon 34141, Republic of Korea
[4]Department of Electrical, Electronics and Communication Engineering, Faculty of Science and Engineering, Tokyo City University, Tokyo 158-8557, Japan

Corresponding author: Watcharapan Suwansantisuk (watcharapan.suw@kmutt.ac.th)

This work was supported in part by the Petchra Pra Jom Klao Ph.D. Research Scholarship from the King Mongkut's University of Technology Thonburi under Grant 54/2563.

ABSTRACT Generalized frequency-division multiplexing (GFDM) is a potential multicarrier scheme for the fifth-generation wireless communication and beyond owing to its advantages over orthogonal frequency-division multiplexing (OFDM). Despite its benefits, GFDM systems are exposed to intercarrier and inter-symbol interferences due to the use of non-orthogonal filters, which make synchronization and channel estimation (CE) in GFDM systems more challenging than those in OFDM systems. Existing work treats frequency synchronization, time synchronization, and CE separately, leading to an accumulation of errors in synchronization, estimation, or both. To address this issue, we propose a method for joint synchronization and CE for GFDM systems. The proposed method employs an optimization strategy that maintains innermost optimization as a least squares (LS) problem. The optimal solution to the LS problem can be expressed explicitly, allowing convenient use in the subsequent steps; specifically, the optimization is performed first in the time synchronization, followed by frequency synchronization, and finally in the CE. In addition, based on the proposed approach, we can derive the Cramer-Rao lower bound (CRLB) exactly, whereas in other schemes, only the approximated CRLB is derived. We compare the performance of the proposed method with that of existing methods using the probability of perfect time synchronization and root mean square error as performance measures. The results reveal that over a wide range of signal-to-noise ratio, the proposed method of joint synchronization and CE improves accuracy and outperforms state-of-the-art methods.

INDEX TERMS Channel estimation, Cramer-Rao lower bound (CRLB), frequency synchronization, GFDM, time synchronization.

I. INTRODUCTION

The third-generation partnership project (3GPP) has developed a standard and introduced several crucial applications for the fifth-generation (5G) communication systems and beyond [1], [2], [3]. These applications have diverse requirements; beyond 5G systems must handle very low latency ranging 10–100 μs, support high mobility of at least 1000 km/h, achieve peak data rates exceeding 1 Tb/s, and allow user devices to receive data at the rate of 1 GB/s [4], [5], [6], [7]. Consequently, the physical layer of 5G wireless communication systems demands high reliability, scalability, flexibility, robustness to fading, and efficient spectrum usage [3], [8].

Orthogonal frequency-division multiplexing (OFDM) has been widely employed as the physical layer in the fourth generation Long-Term Evolution (LTE) wireless technology. However, OFDM has fundamental drawbacks that render it

The associate editor coordinating the review of this manuscript and approving it for publication was Olutayo O. Oyerinde.

unsuitable for 5G communication systems and beyond. The disadvantages include low spectrum efficiency owing to the use of a cyclic prefix (CP) for each OFDM symbol, high out-of-band (OOB) radiation owing to rectangular transmission filters, and a high peak-to-average power ratio (PAPR) to maintain waveform orthogonality [8], [9]. As a result, OFDM will not meet all the demands of the next-generation communication systems.

Several non-orthogonal waveforms have been proposed for next-generation communication. In Faster-than-Nyquist (FTN) signaling [10], symbols are transmitted at a rate higher than the Nyquist rate for a high spectral efficiency at the expense of inter-symbol interference (ISI) and a complex receiver design. Multi-carrier FTN signaling combines the transmitted symbol in both the time and frequency domains to increase the spectral efficiency of one-dimensional FTN signaling [11]. The discrete Fourier transform (DFT) spreading OFDM applies DFT to information-bearing symbols at the transmitter and passes these spread symbols to the inverse DFT of OFDM to achieve an efficient uplink transmission in a coverage-limited area [12], [13]. The unified non-orthogonal waveform (uNOW) expands the transmitter-receiver structure of the DFT spreading OFDM by adding the zeros embedding model and data removal model before and after the DFT block, respectively, to reduce PAPR and increase spectral efficiency [14], [15]. The generalized frequency-division multiplexing (GFDM) is a multicarrier signaling scheme that organizes transmitted symbols into subchannels and subsymbols, and uses a single CP for each block of transmitted symbols to improve spectral efficiency [9]. These next-generation signal schemes provide high transmission rates, but, owing to the intersymbol and intercarrier interference, generally require complex receivers.

The GFDM is considered a promising technique for applications in next-generation communication systems. The key advantage of GFDM lies in its flexibility in both time and frequency domains. Furthermore, GFDM is designed to be flexible and to accommodate high mobility, several transmission and reception modes, heterogeneous devices, and devices operating in multipath-rich environments. It also offers a low PAPR, low OOB radiation, and high spectral efficiency [9], [16]. These benefits have encouraged extensive research into the suitability of GFDM for next-generation communication systems [17].

Despite the benefits offered, GFDM systems face challenges in terms of signal processing. Unlike OFDM transmitters, GFDM transmitters employ non-orthogonal filters, which lead to ISI and intercarrier interference (ICI) and pose challenges to the front-end design of the receiver. The relaxed orthogonality among the subcarriers renders GFDM susceptible to variations in the mobility of the transmitters and receivers. This susceptibility results in a carrier frequency offset (CFO) stemming from the imbalance in the oscillators between the transmitters and receivers, compounded by the Doppler effect. In addition, unlike OFDM, GFDM employs circular filtering. Consequently, the CP, safeguarding only one subsymbol in OFDM, extends its protective scope to encompass multiple subsymbols in GFDM [8]. This characteristic amplifies the sensitivity of GFDM systems to the transmission delays between the transmitter and receiver, leading to symbol time offset (STO). Furthermore, multipaths would impair the channel between the transmitter and receiver. Therefore, channel estimation (CE) is crucial for the accurate decoding of GFDM-modulated symbols and extends use of GFDM in various applications. For example, in beamforming [18], the estimates of the channel gains at each receiving antenna can provide *a priori* probability of the direction of arrival for tracking a millimeter-wave channel. Another example is secrecy transmission from electric vehicles to grids in a heterogeneous network [19], where accurate estimates of channel gains enable optimal relay selection and maximum-ratio combining. To fully realize the advantages of GFDM, therefore, it is essential to synchronize the time and frequency and to estimate the channel accurately.

Time and frequency synchronization and CE in GFDM are challenging, and cannot be handled directly based on the classic methods devised for OFDM. Specifically, the time and frequency synchronization methods for OFDM use the orthogonality of the transmission filter, and thus do not perform well on GFDM, in which non-orthogonal filters are employed. Furthermore, the processes of time synchronization, frequency synchronization, and CE in GFDM systems are highly coupled, owing to the non-orthogonality of the filter.

Some solutions exist for synchronization and CE of GFDM. For example, [20], [21] introduce a CP-based referenceless-estimation approach with a constrained estimation interval. The studies in [21] and [22] present the use of a pseudo-noise (PN) sequence with two identical parts for preamble-assisted STO and CFO estimation. These methods also utilize windowing processes to reduce the OOB radiation. In [2], a triple autocorrelation-based model is proposed and shown to be robust to noise and CFOs. Meanwhile, [23] features a low-complexity CFO estimation method using a preamble with two identical Zadoff-Chu sequences based on the GFDM transmitter structure in [24]. In [2], [21], [22], and [23], CE is assumed to be perfect, and the preamble is restricted to two subsymbols in [21], [22], and [23] for the CFO and STO estimates; however, this approach suffers from issues related to ISI and ICI. The maximum likelihood method described in [25] can be used for referenceless CFO estimation, but the estimation span of the CFO is limited. In [26], a semi-referenceless estimation of the channel and CFO for GFDM is achieved using separate pilot symbols, but at the cost of a high training overhead. The method in [27] utilizes a preamble consisting of multiple identical subsymbols for an efficient CFO estimation. However, the methods in [26] and [27] rely on the assumption of perfect time synchronization, and even under this assumption, these

methods still encounter issues of ISI and ICI. In [28] and [29], mitigation of the distortion induced by nonlinear devices such as high-power amplifiers and analog-to-digital converters is addressed. The method involves preprocessing the received symbols followed by offline training for a low-complexity extreme learning machine (ELM) model. Subsequently, the model is utilized for the STO estimation. In [30], a one-dimensional convolutional neural network (1-D CNN) is introduced to enhance timing accuracy while reducing computational complexity. This approach conceptualizes the time-synchronization problem as a classification problem, where each class corresponds to a potential value of STO. It is noteworthy that the methods in [28], [29], and [30] do not estimate CFO, thus limiting their applicability to a small, negligible CFO. The techniques described above focus on either synchronization alone or synchronization followed by CE separately.

Meanwhile, various solutions for GFDM are concentrated exclusively on CE. Some of these include the GFDM transmission filters in [31], [32], [33], and [34], which are designed to provide pilot-assisted channel estimates that are resilient to interference. However, these filters are only suitable for specific GFDM systems, such as interference-free GFDM or Turbo receivers. In [35], a scattered-pilot-based CE using least squares (LS) is proposed for GFDM systems. However, this technique is affected by ISI and ICI, and involves a large training overhead. An alternative method, the linear minimum mean square error presented in [36], offers a robust CE against ISI and ICI. This method achieves more effective usage of CP by localizing the pilot symbols in GFDM. However, this approach negatively affects the spectral efficiency. In [37], scattered pilots were utilized for CE; however, owing to the underlying assumption of a static channel, this scheme is possibly not suitable for a frequency-selective channel. In [38], a receiver filter was designed to mitigate the impact of the CFO without considering synchronization or CE. In [39] and [40], the orthogonal matching pursuit (OMP) is used for solving LS CE problems. However, the OMP requires knowledge of the channel's physical sparsity, which is difficult to attain. So far, the joint CFO synchronization and channel estimation have been studied under the assumption of perfect time synchronization [7], [41], [42], [43], [44], [45], [46], [47]. However, in practice, this assumption is overly restrictive because obtaining perfect time synchronization is rarely feasible.

Although much work has been done on the synchronization and channel estimation for GFDM systems, the existing studies are limited in fundamental ways in that the CE and synchronization are addressed separately. In the meantime, to accurately estimate the channel, a receiver needs to have correct CFO and STO, which can be obtained only after accurate CE; in short, the tasks of synchronization and CE are coupled and thus should be treated jointly, but not separately as in the existing studies. A method that jointly synchronizes time, synchronizes frequency, and estimates the channel at the same time will lead to transmission reliability and to the full advantages of GFDM transmission.

In this study, we propose a method for the joint synchronization and CE for GFDM. To overcome the complexity of joint synchronization and CE, we formulate an optimization in which common terms appearing repeatedly in the synchronization and CE are identified to avoid redundant computations. The contributions of this study include the following:

- We believe this study is the first to address time and frequency synchronization with the simultaneous estimation of channel gains for GFDM.
- The proposed method addresses the joint estimation of the channel gains, STO, and CFO simultaneously. This approach yields more accurate results than earlier methods that perform estimation and synchronization in a separate sequential manner.
- The performance of the proposed approach is compared with that of the state-of-the-art methods. The comparisons are assessed in terms of root mean square error (RMSE) and Cramer-Rao lower bound (CRLB) for the CFO and CE, and in terms of RMSE and the probability of perfect time synchronization for the STO estimation.

The proposed method is practically useful and applicable to transmitters and receivers that experience frequency offset, time offset, and fading.

The rest of this paper is organized as follows. In Section II, we provide a detailed description of the model of the synchronization and CE for GFDM. In Section III, the proposed method for joint synchronization and CE for GFDM systems is described. In Section IV, after deriving CRLB as an analytical performance metric, we present and discuss the simulation results and compare them with those of other methods. Finally, in Section V, we conclude the study by summarizing the key findings and contributions.

II. SYSTEM MODEL

This section describes the GFDM system in terms of modulation, transmitter, channel, and receiver.

A. GFDM MODULATION

Consider the GFDM modulator shown in Fig. 1, where parallel streams of information-bearing bits enter the modulator and a quadrature amplitude modulation (QAM) is assumed as the mapper. A block of GFDM symbols is composed of $N = KM$ complex numbers and is produced by μM information-bearing bits per stream, where μ is the number of bits encoded at a time into a complex number by the mapper,[1] and K and M denote the numbers of subchannels and subsymbols, respectively. A binary datum or information bit, complex-valued output of the mapper, and GFDM modulated complex-valued vector are denoted

[1]For example, a 4-QAM signal constellation with the expected energy of one maps $\mu = 2$ bits $b_1 b_2$ at a time into a complex number d, where $b_1 b_2 \in \{00, 01, 10, 11\}$ and $d = \frac{1}{\sqrt{2}}\left[(2b_1 - 1) + \tilde{\imath}(2b_2 - 1)\right]$.

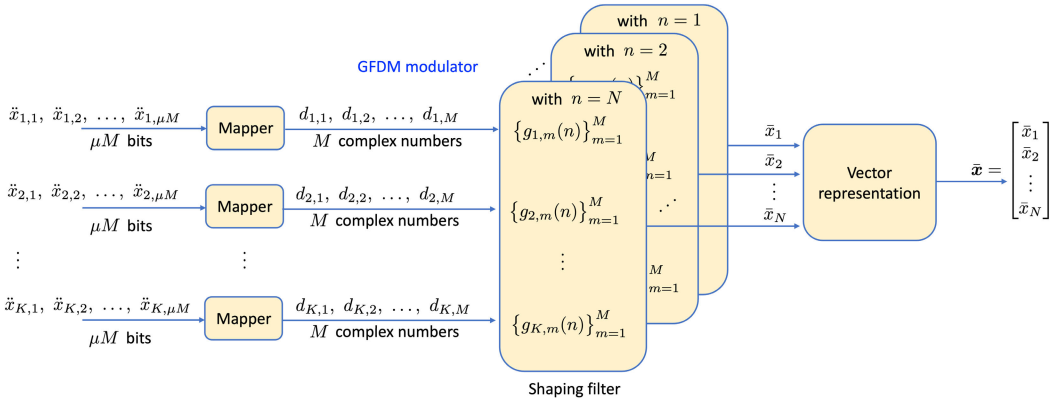

FIGURE 1. A GFDM modulator with K subchannels.

by $\ddot{x}_{ij}$, d_{ijk}, and $\bar{\boldsymbol{x}} = [\bar{x}_1\ \bar{x}_2\ \ldots\ \bar{x}_N]^T$, respectively, where the superscript T denotes a nonconjugate transpose.

The output of the GFDM modulator can then be expressed as

$$\bar{x}_n = \sum_{k=1}^{K}\sum_{m=1}^{M} g_{k,m}(n) d_{k,m} \tag{1}$$

for $n \in \{1, 2, \ldots, N\}$. In (1),

$$g_{k,m}(n) = g\big(\text{mod}\{(n-1)-(m-1)K, N\}\big) \times \zeta_1\big(-(k-1)(n-1)M\big) \tag{2}$$

is[2] a shaping filter [9], [21], [34] with $g(r)$ a GFDM transmission filter function defined for $r \in \{0, 1, \ldots, N-1\}$, $\tilde{\imath} = \sqrt{-1}$,

$$\zeta_\alpha(\ell) = \exp\{\tilde{\imath}\alpha\psi(\ell)\} \tag{3}$$

with

$$\psi(\ell) = 2\pi\frac{\ell}{N}, \tag{4}$$

and the modulo function $\text{mod}\{a, b\}$ denotes the remainder of a when divided by b. Note that OFDM is a special case of GFDM, for which $M = 1$ and $g(r) = 1$ for $r \in \{0, 1, \ldots, N-1\}$. In (1) and (2), the subscripts k and m indicate the subchannel and subsymbol, respectively. Examples of common transmission filter functions include the raised cosine, root raised cosine (RCC), first Xia, and fourth Xia [9].

B. TRANSMITTER

A block diagram of the GFDM transmitter, multipath channel, and receiver is shown in Fig. 2, where K parallel streams of data bits are GFDM-modulated into complex-valued vectors $\bar{\boldsymbol{x}}_1, \bar{\boldsymbol{x}}_2, \ldots$. Each vector $\bar{\boldsymbol{x}}_i$ is of dimension $N \times 1$ and is generated using the procedure shown in Fig. 1 from the data bits $\left\{\{\ddot{x}_{k,j}\}_{j=(i-1)\mu M+1}^{i\mu M}\right\}_{k=1}^{K}$. In addition, an $N \times 1$ dimensional marker block $\bar{\boldsymbol{s}}$, GFDM-modulated from a set $\left\{\{\ddot{s}_{k,j}\}_{j=1}^{\mu M}\right\}_{k=1}^{K}$ of μN bits known to both the transmitter and receiver, is inserted into the sequence $\bar{\boldsymbol{x}}_1, \bar{\boldsymbol{x}}_2, \ldots$ at random position J to aid the receiver for time and frequency synchronization and CE. The resulting sequence is $\tilde{\boldsymbol{x}}_1, \tilde{\boldsymbol{x}}_2, \ldots$, where

$$\tilde{\boldsymbol{x}}_i = \begin{cases} \bar{\boldsymbol{x}}_i, & i \in \{1, 2, \ldots, J-1\}, \\ \bar{\boldsymbol{s}}, & i = J, \\ \bar{\boldsymbol{x}}_{i-1}, & i \in \{J+1, J+2, \ldots\}. \end{cases} \tag{5}$$

Through the operation of CP, cyclic suffix (CS), and windowing, each vector $\tilde{\boldsymbol{x}}_i$ is transformed into a vector

$$\begin{aligned} \boldsymbol{x}_i &= \left[x_{i,1}\ x_{i,2}\ \ldots\ x_{i,N_{\text{ext}}}\right]^T \\ &= \tilde{\boldsymbol{W}}\begin{bmatrix} \boldsymbol{O}_{N_{\text{cp}}\times(N-N_{\text{cp}})} & \boldsymbol{I}_{N_{\text{cp}}} \\ \boldsymbol{I}_N & \\ \boldsymbol{I}_{N_{\text{cs}}} & \boldsymbol{O}_{N_{\text{cs}}\times(N-N_{\text{cs}})} \end{bmatrix}\tilde{\boldsymbol{x}}_i \end{aligned} \tag{6}$$

of size $N_{\text{ext}} \times 1$ with $N_{\text{ext}} = N_{\text{cp}} + N + N_{\text{cs}}$, where N_{cp} and N_{cs} are the lengths of a CP and a CS, respectively; $\boldsymbol{I}_k$ denotes the identity matrix of dimension $k \times k$; $\boldsymbol{O}_{k\times l}$ denotes the all-zero matrix of dimension $k \times l$; and $\tilde{\boldsymbol{W}} = \text{diag}\{w(1), w(2), \ldots w(N_{\text{ext}})\}$ of size $N_{\text{ext}} \times N_{\text{ext}}$ contains the values of a window function $w(\cdot)$ such as the ramp-up ramp-down function [22] or a function identically equal to 1 if no window operation is used. The vectors $\boldsymbol{x}_1, \boldsymbol{x}_2, \ldots$ are transmitted into the communication channel. We again note that the marker frame

$$\begin{aligned} \boldsymbol{s} &= \boldsymbol{x}_J \\ &= \left[s_1\ s_2\ \ldots\ s_{N_{\text{ext}}}\right]^T \end{aligned} \tag{7}$$

plays a key role in the synchronization and channel estimation.

C. CHANNEL AND RECEIVER

The channel is considered to be a fading channel with L resolvable paths and complex-valued zero-mean circularly symmetric Gaussian noise $W(n)$ with a variance of σ^2 per

[2]The right-hand side of (2) is equivalent to (1) in [9].

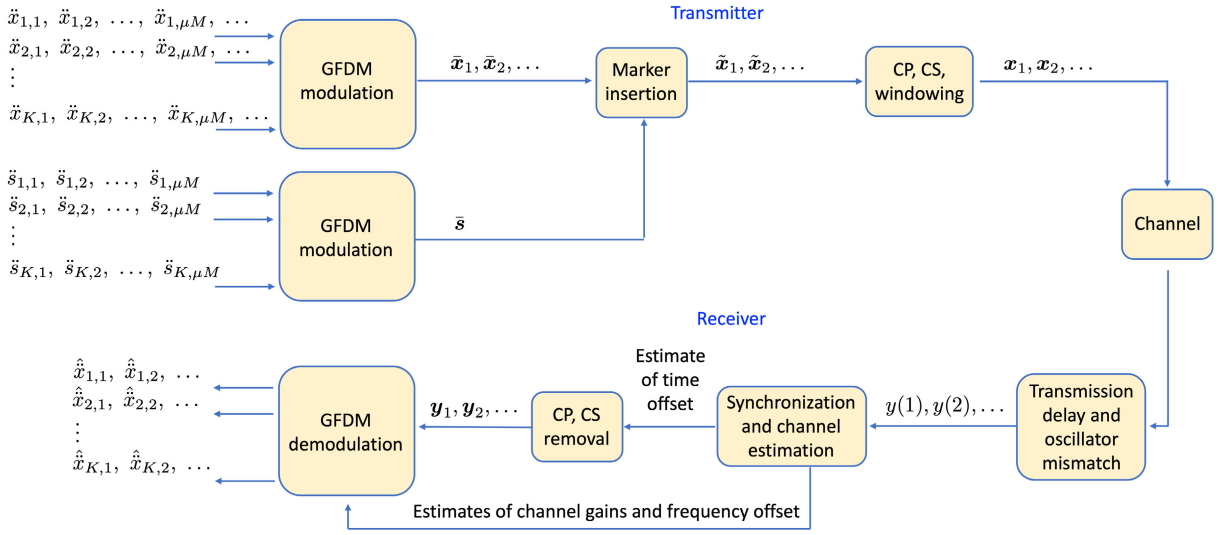

FIGURE 2. A transceiver model of a GFDM system with channel estimation and synchronization.

part. The vector of the channel gains will be denoted by

$$\boldsymbol{h} = [h_1 \; h_2 \; \ldots \; h_L]^T . \tag{8}$$

With the fading, additive noise $W(n)$, STO τ, and CFO ϵ, the received symbols can be expressed as

$$y_{\tau,\epsilon}(n) = \varphi_\epsilon(n-\tau) \sum_{\ell=1}^{L} h_\ell \, x(n-\tau-\ell+1) + W(n). \tag{9}$$

In (9),

$$x(j) = \begin{cases} x_{1+\left\lfloor \frac{j-1}{N_{\text{ext}}} \right\rfloor, 1+\text{mod}(j-1, N_{\text{ext}})}, & j \in \{1, 2, \ldots\} \\ 0, & j \notin \{1, 2, \ldots\}, \end{cases} \tag{10}$$

with the floor function $\lfloor c \rfloor$ denoting the largest integer less than or equal to c, and

$$\varphi_\epsilon(n) = \begin{cases} \zeta_\epsilon\left(\tilde{n}+N\right), & -N_{\text{cp}} \le \tilde{n} \le -1, \\ \zeta_\epsilon\left(\tilde{n}\right), & 0 \le \tilde{n} \le N-1, \\ \zeta_\epsilon\left(\tilde{n}-N\right), & N \le \tilde{n} \le N_{\text{ext}} - N_{\text{cp}} - 1 \end{cases} \tag{11}$$

is the frequency-shift function, which accounts for the effect of CFO in GFDM [48], [49] for $n \in \{1, 2, \ldots, N_{\text{ext}}\}$ and $\tilde{n} = n - 1 - N_{\text{cp}}$. As described by (11), the values of the frequency-shift function form a CP (the first line on the right-hand side of (11)), body (the second line), and CS (the third line) matching a structure of the GFDM frame. Furthermore, (11) also indicates that each one of the N_{ext} symbols in a GFDM frame experiences a frequency shift that is an integer (representing the symbol discrete time) multiple of the CFO ϵ. The $L+2$ parameters $\boldsymbol{h}$, ϵ, and τ are considered constant, but unknown to the receiver. Because ϵ and τ are assumed constants, we drop the subscripts and write $y(\cdot)$ instead of $y_{\tau,\epsilon}(\cdot)$ for notational simplicity.

After receiving a number $N_{\max}$ of symbols $y(1)$, $y(2)$, ..., $y(N_{\max})$, the receiver synchronizes the time and frequency, and estimates the channel. We assume $N_{\max}$ is sufficiently large, such that the entire marker frame $\boldsymbol{s}$ is received. Let I_{ref} denote the reference index, the time index at which the marker frame starts: specifically,

$$I_{\text{ref}} = (J-1)N_{\text{ext}} + 1 + \tau. \tag{12}$$

Then, the received symbols $y(I_{\text{ref}})$, $y(I_{\text{ref}}+1)$, ..., $y(I_{\text{ref}}+N_{\text{ext}}-1)$ correspond to the N_{ext} symbols in the marker frame $\boldsymbol{s}$.

III. PROPOSED METHOD

Let us now propose a method for joint synchronization of time, synchronization of frequency, and estimation of the channel. The primary objective of the proposed method is to estimate the reference time I_{ref}, CFO ϵ, and channel gains $\boldsymbol{h}$ based on the received symbols $y(1)$, $y(2)$, ..., $y(N_{\max})$, and knowledge of the marker symbols via $\boldsymbol{s}$. To search for the marker frame in the received symbol under unknown values of the channel gains, STO, and CFO, we formulate an optimization problem with $L+2$ variables. By efficiently reusing the common terms that appear across several iterations of the algorithm in the joint optimization, an improvement in the performance and speed of the proposed method is attained.

Noting that the value ϵ of the CFO can be considered in the range $\left[-\frac{1}{2}, \frac{1}{2}\right]$ for transmitters and receivers with a small frequency mismatch [21], [26], [50], [51], we formulate the joint optimization of the $L+2$ variables as

$$(\hat{i}, \hat{\epsilon}, \hat{\boldsymbol{h}}) = \arg \min_{i \in \mathcal{U}, \theta \in \left[-\frac{1}{2}, \frac{1}{2}\right], \boldsymbol{\gamma} \in \mathbb{C}^L} f(i, \theta, \boldsymbol{\gamma}), \tag{13}$$

where i, θ, and $\boldsymbol{\gamma} = \begin{bmatrix}\gamma_1 & \gamma_2 & \dots & \gamma_L\end{bmatrix}^T$ are the variables to be optimized;

$$\mathcal{U} = \{1, 2, \dots, N_{\max} - N + 1\} \tag{14}$$

denotes the set of feasible values of i; and $\mathbb{C}^L$ denotes the set of L dimensional complex vectors. In (13), the objective function

$$f(i, \theta, \boldsymbol{\gamma}) = \sum_{n=1}^{N} \left| y(n+i-1) - \zeta_\theta(n-1) v_{\boldsymbol{\gamma}}(n) \right|^2 \tag{15}$$

is the squared difference between the received and marker symbols that passed through a channel and experienced frequency shift. In (15), for $n \in \{1, 2, \dots, N\}$, the term

$$v_{\boldsymbol{\gamma}}(n) = \sum_{\ell=1}^{L} \gamma_\ell \, \check{s}_{n-\ell+1} \tag{16}$$

denotes the convolution between the channel variables $\boldsymbol{\gamma}$ and the marker symbols

$$\begin{aligned} \check{\boldsymbol{s}} &= \begin{bmatrix}\check{s}_{1-N_{\text{cp}}} & \check{s}_{2-N_{\text{cp}}} & \dots & \check{s}_{N+N_{\text{cs}}}\end{bmatrix}^T \\ &= \begin{bmatrix} s_1 & s_2 & \dots & s_{N_{\text{ext}}} \end{bmatrix}^T \end{aligned} \tag{17}$$

after a change of time indices from $\{1, 2, \dots, N_{\text{ext}}\}$ to $\{1 - N_{\text{cp}}, 2 - N_{\text{cp}}, \dots, N + N_{\text{cs}}\}$ for notation convenience: equivalently,

$$\check{s}_i = s_{i+N_{\text{cp}}} \tag{18}$$

for $i \in \{1 - N_{\text{cp}}, 2 - N_{\text{cp}}, \dots, N + N_{\text{cs}}\}$.

The symbols[3] $\hat{i}$, $\hat{\epsilon}$, and $\hat{\boldsymbol{h}}$ denote the estimates of the position of the marker block, the CFO ϵ, and the vector $\boldsymbol{h}$ of channel gains, respectively. Noting that the marker block is appended with a CP of length N_{cp}, the estimate of the reference time can be obtained from the relationship $\hat{I}_{\text{ref}} = \hat{i} - N_{\text{cp}}$.

The feasible sets $\mathbb{C}^L$ and $[-\frac{1}{2}, \frac{1}{2}]$ of $\boldsymbol{\gamma}$ and θ, respectively, are both uncountable. Thus, the optimization in (13) cannot be solved using a naive search. Moreover, the fact that there exist $L+2$ variables in the objective function also complicates the optimization. To address these challenges, we rewrite (13) as

$$(\hat{i}, \hat{\epsilon}, \hat{\boldsymbol{h}}) = \arg\min_{i \in \mathcal{U}} \left(\min_{\theta \in [-\frac{1}{2}, \frac{1}{2}]} \left(\min_{\boldsymbol{\gamma} \in \mathbb{C}^L} f(i, \theta, \boldsymbol{\gamma}) \right) \right). \tag{19}$$

Note in (19) that the innermost optimization can be solved analytically, whereas the outer two optimizations need to be solved iteratively but not analytically.

Specifically, when the variables i and θ are fixed, the solution to the innermost optimization, that is, the estimates

$$\boldsymbol{g}(i, \theta) = \arg\min_{\boldsymbol{\gamma} \in \mathbb{C}^L} f(i, \theta, \boldsymbol{\gamma}) \tag{20}$$

of channel gains can be expressed as [52]

$$\begin{aligned} \boldsymbol{g}(i, \theta) &= \left[\boldsymbol{S}^H \boldsymbol{\Gamma}^H(\theta) \boldsymbol{\Gamma}(\theta) \boldsymbol{S} \right]^{-1} \boldsymbol{S}^H \boldsymbol{\Gamma}^H(\theta) \boldsymbol{y}_{i:i+N-1} \\ &= \boldsymbol{Q}(\theta) \boldsymbol{y}_{i:i+N-1}. \end{aligned} \tag{21}$$

Here,

$$\boldsymbol{Q}(\theta) = \boldsymbol{V} \boldsymbol{\Gamma}^H(\theta) \tag{22}$$

is of size $L \times N$ with the matrix

$$\boldsymbol{V} = \left(\boldsymbol{S}^H \boldsymbol{S} \right)^{-1} \boldsymbol{S}^H \tag{23}$$

of size $L \times N$, $\boldsymbol{y}_{i:j} = [y(i)\ y(i+1)\ \dots\ y(j)]^T$ is a $(j - i + 1) \times 1$ vector of received symbols, the $N \times N$ diagonal matrix

$$\boldsymbol{\Gamma}(\theta) = \text{diag}\left\{ \zeta_\theta(n-1) \,:\, n \in \{1, 2, \dots, N\} \right\} \tag{24}$$

accounts for the CFO variable θ and satisfies

$$\boldsymbol{\Gamma}^H(\theta) \boldsymbol{\Gamma}(\theta) = \boldsymbol{I}_N, \tag{25}$$

and

$$\boldsymbol{S} = \begin{bmatrix} \check{s}_1 & \check{s}_0 & \dots & \check{s}_{2-L} \\ \check{s}_2 & \check{s}_1 & \dots & \check{s}_{3-L} \\ \vdots & \vdots & \ddots & \vdots \\ \check{s}_N & \check{s}_{N-1} & \dots & \check{s}_{N+1-L} \end{bmatrix} \tag{26}$$

is an $N \times L$ matrix of marker symbols. The result (21) is the explicit formula for the estimates of channel gains as a function of i and θ.

Using the solution (21) to the innermost optimization, the optimization problem (19) can be expressed as

$$(\hat{i}, \hat{\epsilon}) = \arg\min_{i \in \mathcal{U}} \left(\min_{\theta \in [-\frac{1}{2}, \frac{1}{2}]} \tilde{f}(i, \theta) \right) \tag{27}$$

$$\hat{\boldsymbol{h}} = \boldsymbol{g}(\hat{i}, \hat{\epsilon}), \tag{28}$$

where

$$\begin{aligned} \tilde{f}(i, \theta) &= f\left(i, \theta, \boldsymbol{g}(i, \theta)\right) \\ &= \left\| \boldsymbol{y}_{i:i+N-1} - \boldsymbol{\Gamma}(\theta) \boldsymbol{S} \boldsymbol{Q}(\theta) \boldsymbol{y}_{i:i+N-1} \right\|^2 \\ &= \left\| \left\{ \boldsymbol{I}_N - \boldsymbol{\Gamma}(\theta) \boldsymbol{S} \boldsymbol{V} \boldsymbol{\Gamma}^H(\theta) \right\} \boldsymbol{y}_{i:i+N-1} \right\|^2 \end{aligned} \tag{29}$$

is the new objective function in the two variables i and θ. Note in (29) that the $N \times N$ matrix $\boldsymbol{S}\boldsymbol{V} = \boldsymbol{S} \left(\boldsymbol{S}^H \boldsymbol{S} \right)^{-1} \boldsymbol{S}^H$ depends only on the marker symbols through $\boldsymbol{S}$ but not on the variables i and θ; this implies that the matrix $\boldsymbol{S}\boldsymbol{V}$ needs to be computed only once, can be reused repeatedly during the optimization process, and consequently provides us with a saving of the running time.

The objective function $\tilde{f}(i, \theta)$ cannot be simplified further. For a fixed i, the mapping $\theta \to \tilde{f}(i, \theta)$ is a function of θ and has in general several local minima because of the matrix $\boldsymbol{\Gamma}(\theta)$, which causes the trigonometric terms $\cos(\theta \psi(n-1))$ and $\sin(\theta \psi(n-1))$ for $n \in \{1, 2, \dots, N\}$ to appear in the objective function. In short, because $\tilde{f}(i, \theta)$ is not a convex function of θ in general, we cannot guarantee that

[3] We use the symbols ϵ, I_{ref}, and $h_1, h_2, \dots, h_L$ for the CFO, reference time, and channel gains. The symbols θ, i, $\gamma_1, \gamma_2, \dots, \gamma_L$ are the variables of the objective function.

Algorithm 1 Joint Synchronization and CE

Require: Received symbols $y(1), y(2), \ldots, y(N_{\max})$; marker symbols via $\boldsymbol{s}$; step size Δ

Ensure: An estimate $\hat{I}_{\text{ref}}$ of the reference index; an estimated CFO $\hat{\epsilon}$; estimates $\hat{\boldsymbol{h}}$ of the channel gains

```
Initialize the value of the objective function to be f* = ∞ and S from š according to (17) and (26)
Compute V = (S^H S)^{-1} S^H and SV
for θ = -1/2 : Δ : 1/2 do
    Initialize Γ(θ) to be the diagonal matrix in (24)
    Initialize Q(θ) = V Γ^H(θ)
    for i = 1 to (N_max - N + 1) do
        Compute f̃(i, θ) according to (29)
        if f̃(i, θ) < f* then
            f* = f̃(i, θ)
            Î_ref = i - N_cp
            ε̂ = θ
            ĥ = Q(θ) y_{i:(i+N-1)}
        end if
    end for
end for
return Î_ref, ε̂, and ĥ
```

the numerical method of optimization finds a minimizer $\hat{\epsilon}$. Thus, we propose using a grid search on variables i and θ to yield estimates of the STO and CFO. With an appropriately chosen step size for θ, the grid search will be a reasonable choice because the variable i belongs to a discrete set $\mathcal{U}$ and the feasible set $\left[-\frac{1}{2}, \frac{1}{2}\right]$ for θ is bounded. An algorithm realizing the proposed method for estimating the STO, CFO, and channel gains is presented in Algorithm 1.

The proposed method shares a similarity with the OMP algorithm outlined in [39] and [40] in that the optimization is solved in part by an LS method. However, a significant difference lies in the channels assumed. The OMP algorithm was designed for sparse multipath channels, whereas the proposed method is applicable to both sparse and dense multipath channels. Moreover, unlike the OMP algorithm, which optimizes two parameters, namely the STO and channel gains, the proposed method optimizes three parameters: STO, CFO, and channel gains.

In Algorithm 1, after the variables are initialized and the constant terms are computed, the process is iterated over the set $\left\{-\frac{1}{2} + k\Delta \ : \ k \text{ is an integer such that } 0 \leq k \leq \frac{1}{\Delta}\right\}$ of θ. For each θ, the algorithm evaluates and reuses the term $\boldsymbol{Q}(\theta) = \boldsymbol{V}\boldsymbol{\Gamma}^H(\theta)$ for every iteration of variable i. During this process, Algorithm 1 efficiently implements the optimization in (27) by reusing the common terms throughout the iteration in i. If the value of the current objective function is smaller than the previously known minimal value, the algorithm updates the estimates of STO, CFO, and channel gains. The algorithm continues until all combinations of the time index and CFO are exhausted. The algorithm terminates and returns the estimates of the time offset, CFO, and channel gains.

The running time complexity is primarily derived from the iteration in θ, iteration in i, and multiplication of the $N \times N$ matrix $\boldsymbol{\Gamma}(\theta)\boldsymbol{S}\boldsymbol{V}\boldsymbol{\Gamma}^H(\theta)$ with an $N \times 1$ vector $\boldsymbol{y}_{i:i+N-1}$ when computing $\tilde{f}(i, \theta)$. The running time complexity of the proposed method implemented via Algorithm 1 is $O\left(\frac{N_{\max}N^2}{\Delta}\right)$; considering that the number $N_{\max}$ of symbols can typically be approximated by a constant multiplication of N, the running time complexity is $O\left(\frac{N^3}{\Delta}\right)$, which depends on the search resolution Δ of the CFO. As Δ decreases, the number of iterations for searching for CFO increases, and the numerical estimate of CFO becomes more accurate at the expense of a longer running time. The selection of Δ should be balanced between the accuracy and complexity. As a rule of thumb, we recommend $\Delta = 10^{-2}$ or less, meaning that the estimate of CFO is accurate by at least two decimals. For a fixed choice of Δ, the running time complexity of the proposed method grows with N^3, which is moderate for a typical block length N.

For the twofold-symmetric-block [22, Eq. (27)], fourfold-symmetric-block [53] with coarse estimation, fourfold-symmetric-block with fine estimation, PN-based method, and CP-based method [21], the running time complexities are $O(N_{\max}N)$, $O(N_{\max} + N)$, $O(N_{\max} + N_{\text{cp}}N)$, $O(N_{\max}N)$, and $O(N_{\max}N_{\text{cp}})$, respectively. The state-of-the-art methods run faster than the proposed method by at least a factor of N, partly because they do not jointly synchronize time, synchronize frequency, and estimate the channel. However, as will become apparent in the next section, the state-of-the-art methods are less accurate than the proposed method.

IV. PERFORMANCE EVALUATION

In this section, we evaluate the synchronization and CE performance of the proposed method. We also compare the performance with that of state-of-the-art methods. In the comparison of synchronization, we consider five state-of-the-art methods: the twofold-symmetric-block method [22], PN-based method [21, Sec. IV], CP-based method [21, Sec. III], fourfold-symmetric-block [53, Sec. III.A] with coarse estimation, and fourfold-symmetric-block with fine estimation [53, Sec. III.B] denoted by SB2, PN-based, CP-based, SB4-C, and SB4-F, respectively. In the comparison of the performance of CE, we have considered the correlation-based method of the fourfold-symmetric-block with fine STO estimation, also denoted by SB4-F. In addition, we also compare the proposed method with the separate processing of LS CE after synchronization.

The performance metrics are the probability[4] of perfect time synchronization and RMSE in the STO estimation, and the RMSE in the CFO estimation and CE. In this section,

[4]The probability $\mathbb{P}\left\{\hat{I}_{\text{ref}} = I_{\text{ref}}\right\}$ of perfect time synchronization is defined as the probability that the estimated reference index is equal to the actual reference index. This probability is approximated numerically by the ratio $\frac{1}{N_T}\sum_{n=1}^{N_T}\mathbb{I}\{\hat{I}_n = I_{\text{ref}}\}$, where N_T is the number of simulation rounds, $\hat{I}_n$ is the estimate of the reference time at the n^{th} simulation round, and $\mathbb{I}$ is the indicator function.

TABLE 1. Values of parameters in the simulation and channel modeling.

Parameter	Value
Length of GFDM block (N)	512
Number of GFDM subsymbols (M) for the	
proposed	4
fourfold-symmetric-block	4
twofold-symmetric-block	2
PN-based	2
CP-based	4
methods	
Number of GFDM subcarriers (K) for the	
proposed	128
fourfold-symmetric-block	128
twofold-symmetric-block	256
PN-based	256
CP-based	128
methods	
Modulation scheme	4-QAM
Modulation order (μ)	2
Length of the CP (N_{cp})	32
Length of the CS (N_{cs})	0
Frame length of GFDM (N_{ext})	544
Transmission filter	
type	RCC
roll-off factor	0.75
Number of channel taps (L)	4
Power delay profile	
type	exponential
decay factor	0.8
Fading distribution	Rayleigh
Normalized SNR	-10 to 5 dB
Search resolution (Δ)	0.01
Number of received symbols ($N_{\max}$)	2176

we employ the normalized signal-to-noise ratio (SNR), defined as $10\log_{10}\frac{1}{\sigma^2} = -10\log_{10}\sigma^2$ assuming 1 for the signal power per part. The values of the parameters used in the simulations are listed in Table 1. Each point in the figures provided in this section was obtained via 2000 iterations, except for the CRLB, which was obtained using numerical methods.

A. STO ESTIMATION

Fig. 3 illustrates the probability $\mathbb{P}\left\{\hat{I}_{\text{ref}} = I_{\text{ref}}\right\}$ of perfect time synchronization for the proposed method, SB2, PN-based, CP-based, SB4-C, and SB4-F when $\epsilon = 0.2$ and 0.4. Note here that both $\hat{I}_{\text{ref}}$ and I_{ref} are integers. The proposed method is observed to consistently achieve a probability of perfect time synchronization higher than that of the other methods over a wide range of normalized SNR. In addition, the proposed method shows robustness to the change of the CFO and, when the CFO is larger, provides a higher gain especially over SB4-C and SB4-F. For instance, at SNR$= -5$ dB, the probabilities of perfect time synchronization are approximately 0.83, 0.68, 0.42, 0.10, 0.48, and 0.15 for the proposed method, SB2, PN-based, CP-based, SB4-F, and SB4-C, respectively, when $\epsilon = 0.2$; the values are approximately 0.82, 0.67, 0.42, 0.10, 0.13, and 0.02, respectively, when $\epsilon = 0.4$. The superior performance of the proposed method is due to a smaller accumulated synchronization error resulting from the combined procedure in the proposed method.

In Fig. 4, the probability of perfect time synchronization is demonstrated over the entire range of CFO at two normalized SNR levels: a low normalized SNR level of -5 dB and a moderate normalized SNR level of 0 dB. At a normalized SNR of -5 dB, the proposed method achieves a probability of perfect time synchronization of approximately 0.83, which is higher by approximately 0.15, at least 0.40, at least 0.80, at least 0.25, and at least 0.65 than those of SB2, PN-based, CP-based, SB4-F, and SB4-C, respectively. A similar observation, except that the margins decrease slightly, can be made when the normalized SNR is 0 dB. It is also observed that the probabilities of perfect time synchronization of the proposed method, PN-based, CP-based, and SB2 are robust to the variation in CFO. In general, Fig. 4 clearly demonstrates that the proposed method is more robust to CFO and surpasses the state-of-the-art methods in achieving precise time synchronization.

Fig. 5 shows the RMSE, normalized by the maximum, between the estimated and actual STOs. Here, the normalization onto the interval [0, 1] is adopted to ensure fairness when comparing the CP-based method, which estimates the CP position, and other methods, which estimate the marker position [49, Appendix B]. It is observed that all the methods exhibit a decreasing normalized RMSE as the SNR increases. In addition, the RMSEs of PN-based, CP-based, and SB2 do not depend on the variation in CFO, whereas those of SB4-F and SB4-C are sensitive to the variation in CFO.

B. ANALYSIS OF CE PERFORMANCE

The mean square error (MSE) $\mathbb{E}\left\{\left|\hat{h}_\ell - h_\ell\right|^2\right\}$ of an unbiased estimator $\hat{h}_\ell$ of the channel gain h_ℓ and the MSE $\mathbb{E}\left\{\left|\hat{\epsilon} - \epsilon\right|^2\right\}$ of an unbiased estimator $\hat{\epsilon}$ of the CFO ϵ satisfy

$$\mathbb{E}\left\{\left|\hat{h}_\ell - h_\ell\right|^2\right\} \geq H_{\ell,\ell} + H_{L+\ell,L+\ell} \tag{30}$$

for $\ell \in \{1, 2, \ldots, L\}$, and

$$\mathbb{E}\left\{\left|\hat{\epsilon} - \epsilon\right|^2\right\} \geq H_{2L+1,2L+1}, \tag{31}$$

respectively. Here, $H_{i,j}$ denotes the element in row i and column j of the inverse of the $(2L+1)\times(2L+1)$ Fisher information matrix $\boldsymbol{F}_{\boldsymbol{\Theta}}$ described via (36) in Appendix with

$$\boldsymbol{\Theta} = \left[h_1^{\text{R}}\ h_2^{\text{R}}\ \ldots\ h_L^{\text{R}}\ h_1^{\text{I}}\ h_2^{\text{I}}\ \ldots\ h_L^{\text{I}}\ \epsilon\right]^T, \tag{32}$$

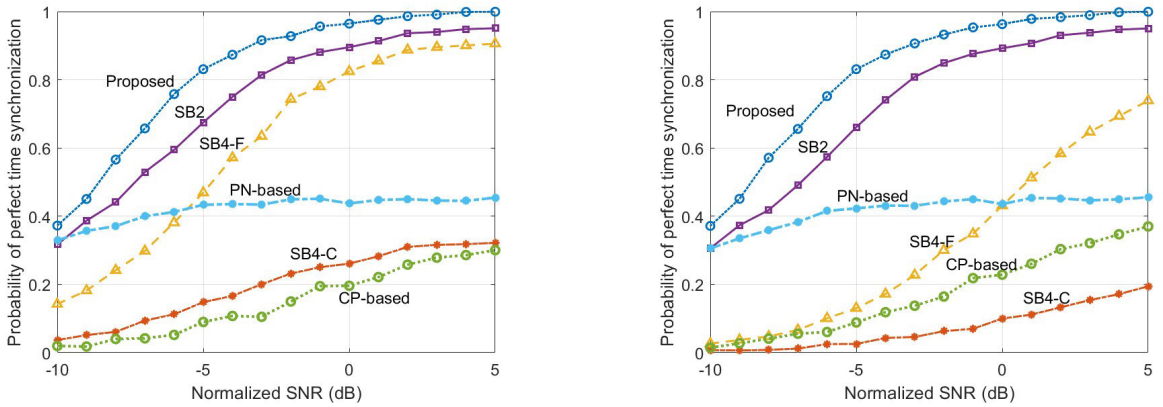

(a) $\epsilon = 0.2$ (b) $\epsilon = 0.4$

FIGURE 3. Probability of perfect time synchronization of several methods as a function of SNR.

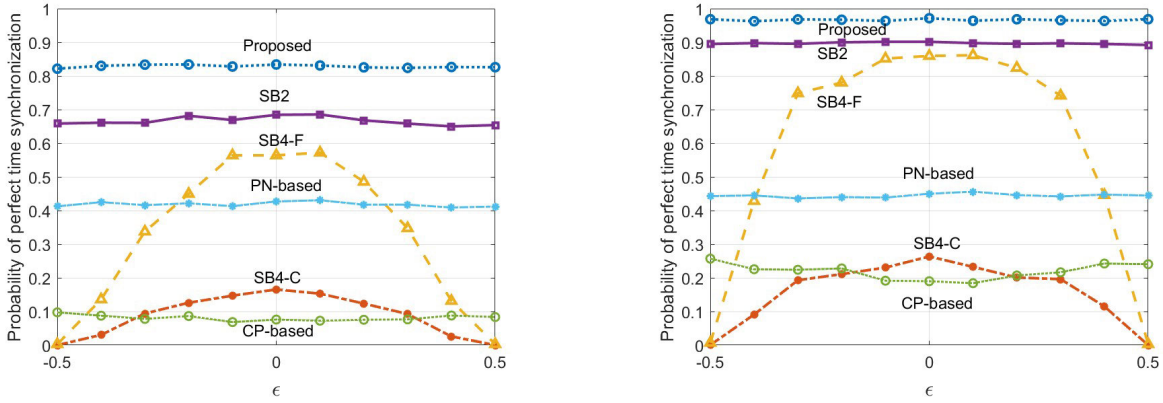

(a) Normalized SNR $= -5$ dB (b) Normalized SNR $= 0$ dB

FIGURE 4. Probability of perfect time synchronization of several methods as a function of the CFOs.

a vector of size $(2L+1)\times 1$. In (32), the superscripts R and I represent the real and imaginary parts, respectively. In short, inequalities (30) and (31) represent the ultimate performance limits of any unbiased estimator of the channel gains and CFO, respectively.

Comparing the performance of the proposed method to the CRLB provides valuable insights into how closely the performance of the proposed method approaches the theoretical bound, thereby validating the effectiveness of the proposed method and its potential applicability in practical communication scenarios. In Fig. 6, the RMSEs of the estimates of the channel gains $\{h_\ell\}_{\ell=1}^{4}$ for the four paths from the proposed, SB4-F, and LS methods are shown, Fig. 6(a) when $\epsilon = 0.2$ and Fig. 6(b) when $\epsilon = 0.4$. The proposed method synchronizes the time and frequency and estimates the channel jointly, whereas the SB4-F and LS methods perform these two processes serially. In the implementation of the LS method, we use the SB2 method for synchronization and the linear LS method for channel estimation. It is observed in both figures that the RMSE of the channel estimates from the proposed method is relatively low, does not depend much on the CFO, and, as the SNR increases, becomes lower than those obtained by the SB4-F and LS methods, and approaches the CRLB. The proposed method, which performs joint synchronization and CE, is superior to the SB4-F and LS methods, which perform these operations sequentially.

C. CFO ESTIMATION

In Fig. 7, the performance of the proposed method for the CFO estimation is compared with that of state-of-the-art methods and CRLB, in Fig. 7(a) when $\epsilon = 0.2$ and in Fig. 7(b) when $\epsilon = 0.4$. In both figures, the RMSEs of SB4-C and SB4-F are almost indistinguishable. For SB2 and PN-based, the CFO is estimated using the phase angle of the correlation between two identical parts of the GFDM symbols acting as a marker block. In the CP-based method, the CP that appears before a block of GFDM symbols is used for CFO estimation. The SB4-C and SB4-F estimate the CFO using the phase angle of the correlation between

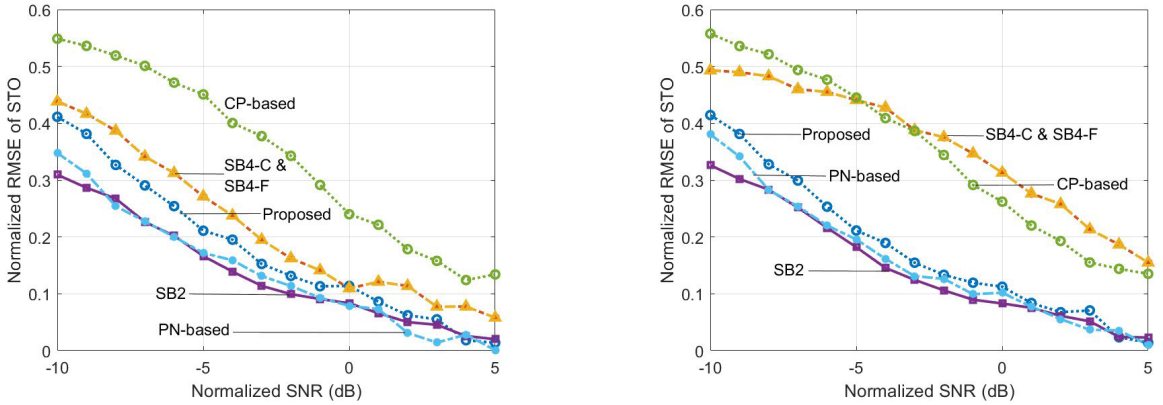

(a) $\epsilon = 0.2$ (b) $\epsilon = 0.4$

FIGURE 5. The RMSE of STO estimates of several methods.

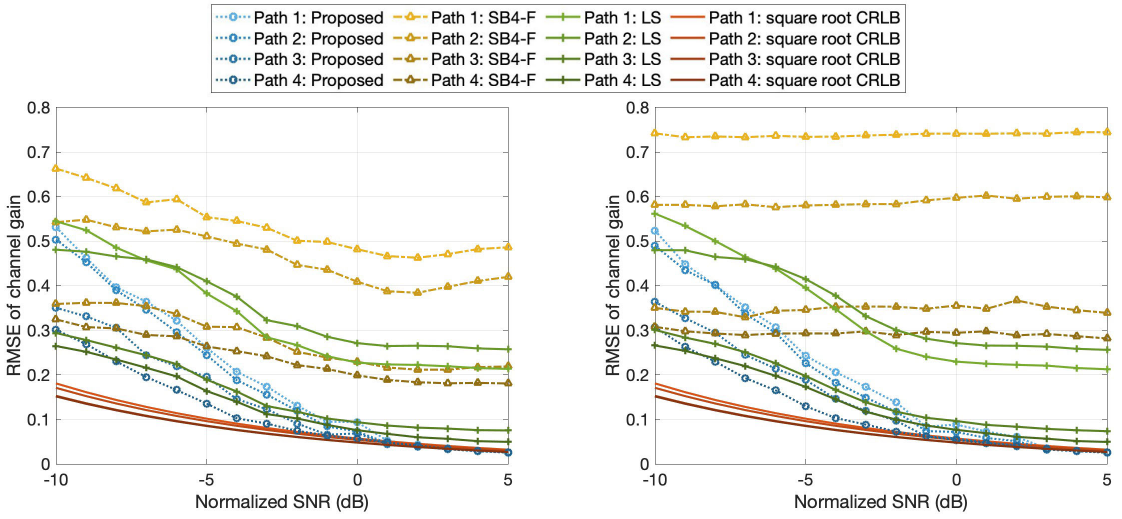

(a) $\epsilon = 0.2$ (b) $\epsilon = 0.4$

FIGURE 6. The RMSE of the channel estimates of three methods as a function of SNR.

the complementary pair sequence of the GFDM block, which also functions as a marker block. It is clearly observed that the proposed method, as well as the other state-of-the-art methods, exhibit a decreasing RMSE as the normalized SNR increases, except the CP-based method, which has a constant estimation error across the entire range of the SNR. In Fig. 7(a), it is also observed that the proposed method, SB4-C, and SB4-F provide almost the same performance, yet outperform SB2, PN-based, and CP-based except when the SNR is high. On the other hand, Fig. 7(b) shows us that when the CFO is larger, the proposed method outperforms all the other methods and maintains the gain over a wider range of the SNR.

In Fig. 7(a), at the normalized SNR of -10 dB, the RMSEs of the SB4-C, SB4-F, and CP-based methods are approximately equal to ϵ because these methods synchronize the time first, and then calculate the correlation to estimate the CFO.[5] When the time synchronization is in error for these methods (as shown in Fig. 3(a) at -10 dB), their CFO estimates are approximately zero because the correlation takes place between two blocks of random symbols. As a consequence, the RMSEs for the estimates of the CFO of the SB4-C, SB4-F, and CP-based methods are approximately $\sqrt{(\epsilon - \hat{\epsilon})^2} = \epsilon$ with $\hat{\epsilon} = 0$ when the SNR is low. Therefore, when the SNR is low and ϵ is small, the SB4-C, SB4-F, and CP-based methods produce an RMSE smaller than that of the proposed method. On the other hand, as observed in Fig. 7(b) and in previous figures also, the proposed method is less sensitive to the change of ϵ than SB4-C, SB4-F, and CP-based methods, and clearly performs better than the other methods except when ϵ is small.

[5]Recall that the SB4-C, SB4-F, and CP-based methods estimate the CFO to be the phase angle of a complex-valued correlation, divided by a constant.

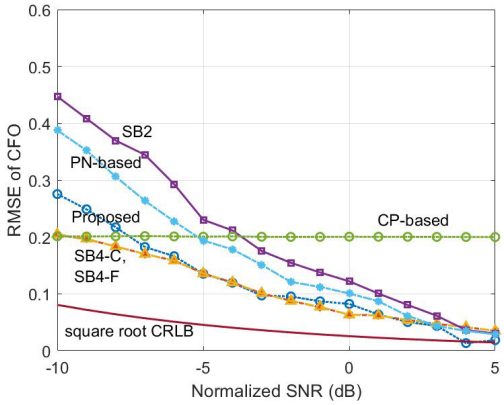

(a) $\epsilon = 0.2$

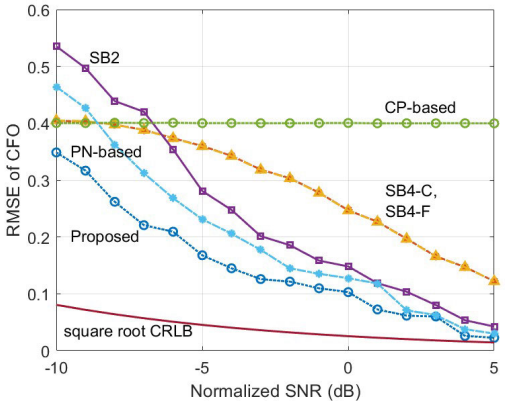

(b) $\epsilon = 0.4$

FIGURE 7. The RMSE of CFO estimates of four methods.

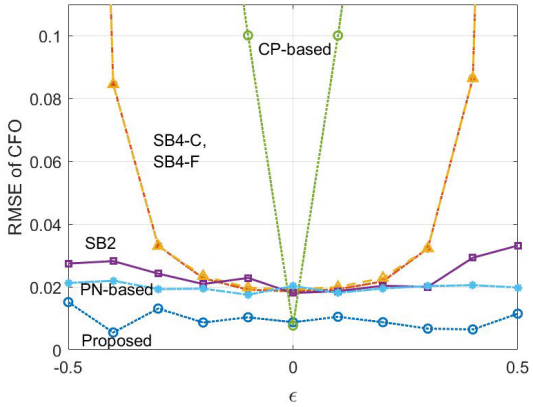

FIGURE 8. The RMSE of the CFO estimates at the normalized SNR of 5 dB.

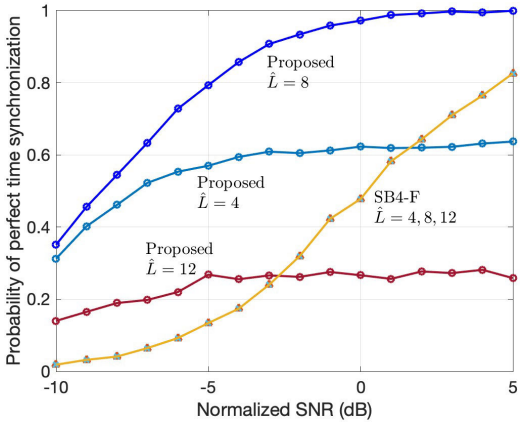

FIGURE 9. Probability of perfect time synchronization when $(L, \hat{L})$ equal to (8, 4), (8, 8), and (8, 12).

In Fig. 8, the RMSEs of the CFO estimates for the six methods are shown over the entire range $[-0.5, 0.5]$ of the CFO when the normalized SNR is 5 dB. This figure again indicates that the proposed method outperforms the other methods over the entire range of the CFO. Specifically, the proposed method provides an RMSE lower than those of SB2 and PN-based methods by a factor of 2 over the entire range of the CFO. In addition, the RMSE of the CFO estimates from the proposed method is approximately half that from SB4-C and SB4-F when the CFO is in the range $[-0.2, 0.2]$ and the ratio becomes even smaller outside this range. It should be noted for fairness that, unlike the proposed, SB2, and SB4-F methods, the CP-based and SB4-C methods employ referenceless estimation without assuming the availability of known marker values.

D. ROBUSTNESS TO ERROR IN NUMBER OF PATHS

This section evaluates the influence of incorrect information about the number L of propagation paths on the performance of two synchronization and CE methods, namely, the proposed and SB4-F methods. We fixed the CFO at a moderate value $\epsilon = 0.4$. For the exponential delay profile, a decay factor of 0.2 is assumed to ensure a sufficient signal energy at the weakest propagation path. Let $\hat{L}$ denote the number of propagation paths used by the receiver when performing the synchronization and CE, which is not necessarily equal to the actual number L of propagation paths. We consider simulation scenarios for $(L, \hat{L}) = (8, 4)$, $(8, 8)$, and $(8, 12)$. These simulation scenarios cover cases in which the number of paths used in the receiver for the synchronization and CE is smaller than, equal to, or larger than the actual number of paths.

Figs. 9 and 10 present the probability of perfect time synchronization and RMSE of the STO, respectively. Fig. 9 shows that the synchronization performance of the proposed method deteriorates when an incorrect number of propagation paths is used at the receiver of the proposed method. Note that the probability of perfect time synchronization of the SB4-F method does not depend on $\hat{L}$ because we implemented the fine-search threshold according to [53, eq. (25)] by assuming

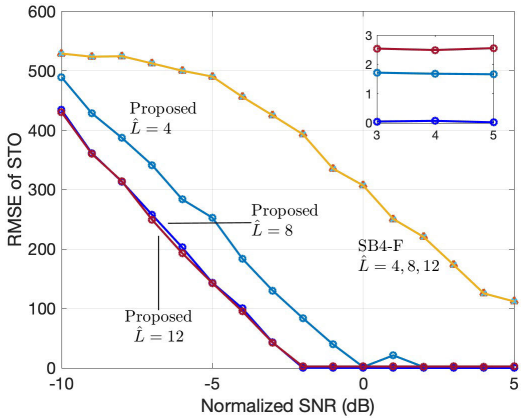

FIGURE 10. The RMSE of the STO estimates when $(L, \hat{L})$ equal to (8, 4), (8, 8), and (8, 12).

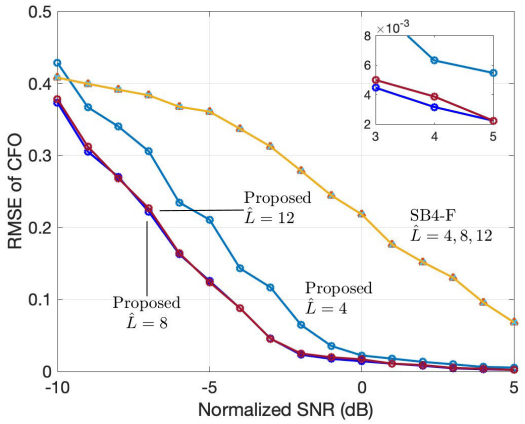

FIGURE 11. The RMSE of the CFO estimates when $(L, \hat{L})$ equal to (8, 4), (8, 8), and (8, 12).

a perfectly known received SNR for the SB4-F method. In Fig. 10, it is clearly observed that the proposed method produces a uniformly smaller RMSE than the SB4-F method over the entire range of the SNR even when an incorrect number of propagation paths is assumed at the receiver.

Fig. 11 shows the RMSE of the CFO under the simulation scenarios $(L, \hat{L}) = (8, 4)$, $(8, 8)$, and $(8, 12)$. It is again observed that, even with the incorrect information on the number of propagation paths, the proposed method outperforms the SB4-F in terms of the CFO synchronization virtually over the entire range of the SNR.

The SB4-F method seems to be less sensitive to errors in the number of propagation paths as long as the SNR needed to calculate the fine-search threshold is available exactly. Although the probability of perfect time synchronization of the proposed method is dependent on $\hat{L}$, the proposed method is superior to the SB4-F method in terms of the RMSEs of STO and CFO over a wide range of the SNR.

V. CONCLUDING REMARK

In this section, we discuss and summarize important findings.

A. DISCUSSION

The proposed method of the joint synchronization and estimation for GFDM systems benefits from the various elements that enhance its accuracy. The proposed method utilizes joint optimization and a refined formulation of the objective function, which reduces complexity when exploring the optimal time and frequency values. The optimization approach employed in the proposed method ensures that the innermost optimization remains an LS problem. After analytically obtaining the conditional solution, that is, the channel gains as functions of STO and CFO, for the LS problem, the optimization problem is solved by iteration. Unlike other methods, in which errors tend to accumulate over the steps, the error does not accumulate in the proposed method, contributing to the enhancement in the accuracy of the synchronization and estimation. In essence, several components are combined, resulting in an improved performance of the proposed method.

B. SUMMARY

This study investigated a scheme for the joint synchronization of time, synchronization of frequency, and estimation of channel gains for GFDM systems. The proposed method utilized LS estimation approach with iterative steps in the joint synchronization and estimation. The performance of the proposed method was verified through simulations, which showed a higher probability of perfect time synchronization compared to the other methods. In addition, the proposed method was shown to incur a lower RMSE over a wide range of SNR for both the CFO and channel gain estimates compared to other methods. As synchronization and channel estimation need to be achieved precisely before digital receivers decode data, joint synchronization and channel estimation could be useful also for other next-generation signaling schemes, such as DFT spreading OFDM, multi-carrier FTN, and uNOW. An open challenge for future research is to design a joint synchronization and CE method for these signaling schemes.

APPENDIX

DERIVATION OF THE CRLB

Let $\boldsymbol{A} = [A_1\ A_2\ \ldots\ A_N]^T$ and $\boldsymbol{B} = [B_1\ B_2\ \ldots\ B_N]^T$, where A_n and B_n are the real and imaginary parts, respectively, of $y(I_{\text{ref}} + N_{\text{cp}} - 1 + n)$ for $n \in \{1, 2, \ldots, N\}$. Then, the joint probability density function (PDF) of $\boldsymbol{A}$ and $\boldsymbol{B}$ can be expressed as

$$f_{\boldsymbol{A},\boldsymbol{B}}(\boldsymbol{a}, \boldsymbol{b}) = \prod_{n=1}^{N} \left\{ f_{p_n(\boldsymbol{\Theta});\sigma^2}(a_n) f_{q_n(\boldsymbol{\Theta});\sigma^2}(b_n) \right\}. \tag{33}$$

In (33), $f_{\alpha;\beta}(x)$ denotes the normal PDF with mean α and variance β; $p_n(\boldsymbol{\Theta})$ and $q_n(\boldsymbol{\Theta})$ denote the real and imaginary parts, respectively, of $v_{\boldsymbol{h}}(n) = \zeta_\epsilon(n-1) \sum_{\ell=1}^{L} h_\ell \check{s}_{n-\ell+1}$; $\boldsymbol{a} = [a_1\ a_2\ \ldots\ a_N]^T$; and $\boldsymbol{b} = [b_1\ b_2\ \ldots\ b_N]^T$. Substituting the expressions of normal PDFs into (33), taking the natural logarithm, and simplifying the terms, we can obtain the log-

likelihood function

$$\Lambda(\boldsymbol{a},\boldsymbol{b};\boldsymbol{\Theta}) = -N\ln(2\pi\sigma^2) - \frac{1}{2\sigma^2}\sum_{n=1}^{N}\Big[\{a_n - p_n(\boldsymbol{\Theta})\}^2 + \{b_n - q_n(\boldsymbol{\Theta})\}^2\Big]. \tag{34}$$

It is well-known [7], [54] that the covariance matrix $\mathbb{E}\left\{\left(\hat{\boldsymbol{\Theta}}-\boldsymbol{\Theta}\right)\left(\hat{\boldsymbol{\Theta}}-\boldsymbol{\Theta}\right)^T\right\}$ of any unbiased estimator $\hat{\boldsymbol{\Theta}}$ of $\boldsymbol{\Theta}$ satisfies the inequality

$$\mathbb{E}\left\{\left(\hat{\boldsymbol{\Theta}}-\boldsymbol{\Theta}\right)\left(\hat{\boldsymbol{\Theta}}-\boldsymbol{\Theta}\right)^T\right\} \geq \boldsymbol{F}_{\boldsymbol{\Theta}}^{-1}, \tag{35}$$

where $\boldsymbol{F}_{\boldsymbol{\Theta}}$ is the Fisher information matrix of dimension $(2L+1)\times(2L+1)$ and the notation $\boldsymbol{A} \geq \boldsymbol{B}$ indicates that the matrix $\boldsymbol{A}-\boldsymbol{B}$ is positive semidefinite: the positive semidefiniteness in (35) implies eventually element-wise inequalities for diagonal elements.

The element in row i and column j of $\boldsymbol{F}_{\boldsymbol{\Theta}}$ is given by the derivative of the log-likelihood function as

$$F_{\boldsymbol{\Theta},i,j} = -\mathbb{E}\left\{\frac{\partial^2\Lambda(\boldsymbol{A},\boldsymbol{B};\boldsymbol{\Theta})}{\partial\Theta_i\partial\Theta_j}\right\}, \tag{36}$$

where Θ_j denotes the jth element of $\boldsymbol{\Theta}$. By substituting the right-hand side of (34) into (36); replacing a_n and b_n with random variables A_n and B_n, respectively; taking the partial derivative; applying the linearity of the expected value; and noting that $\mathbb{E}\{A_n\} = p_n(\boldsymbol{\Theta})$ and $\mathbb{E}\{B_n\} = q_n(\boldsymbol{\Theta})$, we can rewrite (36) into

$$F_{\boldsymbol{\Theta},i,j} = \frac{1}{\sigma^2}\sum_{n=1}^{N}\left\{\frac{\partial p_n(\boldsymbol{\Theta})}{\partial\Theta_i}\frac{\partial p_n(\boldsymbol{\Theta})}{\partial\Theta_j} + \frac{\partial q_n(\boldsymbol{\Theta})}{\partial\Theta_i}\frac{\partial q_n(\boldsymbol{\Theta})}{\partial\Theta_j}\right\}. \tag{37}$$

Explicit expressions of the partial derivatives in (37) can be obtained easily as

$$\frac{\partial p_n(\boldsymbol{\Theta})}{\partial\Theta_i} = \begin{cases} \mathrm{Re}\left\{\zeta_\epsilon(n-1)\check{s}_{n-i+1}\right\}, & 1\leq i\leq L,\\ -\mathrm{Im}\left\{\zeta_\epsilon(n-1)\check{s}_{n-i+L+1}\right\}, & L+1\leq i\leq 2L,\\ -\psi(n-1)q_n(\boldsymbol{\Theta}), & i=2L+1, \end{cases} \tag{38}$$

and

$$\frac{\partial q_n(\boldsymbol{\Theta})}{\partial\Theta_i} = \begin{cases} \mathrm{Im}\left\{\zeta_\epsilon(n-1)\check{s}_{n-i+1}\right\}, & 1\leq i\leq L,\\ \mathrm{Re}\left\{\zeta_\epsilon(n-1)\check{s}_{n-i+L+1}\right\}, & L+1\leq i\leq 2L,\\ -\psi(n-1)p_n(\boldsymbol{\Theta}), & i=2L+1. \end{cases} \tag{39}$$

The CRLBs, the right-hand sides of (30) and (31), can subsequently be evaluated via numerical methods for matrix inversion.

REFERENCES

[1] S. Rostami, P. Kela, K. Leppanen, and M. Valkama, "Wake-up radio-based 5G mobile access: Methods, benefits, and challenges," *IEEE Commun. Mag.*, vol. 58, no. 7, pp. 14–20, Jul. 2020.

[2] D. Wang, Z. Mei, H. Zhang, and H. Li, "A novel PSS timing synchronization algorithm for cell search in 5G NR system," *IEEE Access*, vol. 9, pp. 5870–5880, 2021.

[3] G. Noh, J. Kim, S. Choi, N. Lee, H. Chung, and I. Kim, "Feasibility validation of a 5G-enabled mmWave vehicular communication system on a highway," *IEEE Access*, vol. 9, pp. 36535–36546, 2021.

[4] T. S. Rappaport, Y. Xing, O. Kanhere, S. Ju, A. Madanayake, S. Mandal, A. Alkhateeb, and G. C. Trichopoulos, "Wireless communications and applications above 100 GHz: Opportunities and challenges for 6G and beyond," *IEEE Access*, vol. 7, pp. 78729–78757, 2019.

[5] Z. Zhang, Y. Xiao, Z. Ma, M. Xiao, Z. Ding, X. Lei, G. K. Karagiannidis, and P. Fan, "6G wireless networks: Vision, requirements, architecture, and key technologies," *IEEE Veh. Technol. Mag.*, vol. 14, no. 3, pp. 28–41, Sep. 2019.

[6] M. Ataeeshojai, R. C. Elliott, W. A. Krzymien, C. Tellambura, and J. Melzer, "Energy-efficient resource allocation in single-RF load-modulated massive MIMO HetNets," *IEEE Open J. Commun. Soc.*, vol. 1, pp. 1738–1764, 2020.

[7] A. Mohammadian and C. Tellambura, "Joint channel and phase noise estimation and data detection for GFDM," *IEEE Open J. Commun. Soc.*, vol. 2, pp. 915–933, 2021.

[8] I. B. F. de Almeida, L. L. Mendes, J. J. P. C. Rodrigues, and M. A. A. da Cruz, "5G waveforms for IoT applications," *IEEE Commun. Surveys Tuts.*, vol. 21, no. 3, pp. 2554–2567, 3rd Quart., 2019.

[9] N. Michailow, M. Matthé, I. S. Gaspar, A. N. Caldevilla, L. L. Mendes, A. Festag, and G. Fettweis, "Generalized frequency division multiplexing for 5th generation cellular networks," *IEEE Trans. Commun.*, vol. 62, no. 9, pp. 3045–3061, Sep. 2014.

[10] T. Ishihara, S. Sugiura, and L. Hanzo, "The evolution of faster-than-Nyquist signaling," *IEEE Access*, vol. 9, pp. 86535–86564, 2021.

[11] Y. Ma, N. Wu, J. A. Zhang, B. Li, and L. Hanzo, "Generalized approximate message passing equalization for multi-carrier faster-than-Nyquist signaling," *IEEE Trans. Veh. Technol.*, vol. 71, no. 3, pp. 3309–3314, Mar. 2022.

[12] A. Sahin, E. Bala, R. Yang, and R. L. Olesen, "DFT-spread OFDM with frequency domain reference symbols," in *Proc. IEEE Global Commun. Conf.*, Dec. 2017, pp. 1–6.

[13] K. R. Gudimitla, M. S. A. Khan, S. Amuru, and K. Kuchi, "Pre-DFT multiplexing of reference signals and data in DFT-s-OFDM systems," *IEEE Open J. Commun. Soc.*, vol. 5, pp. 514–525, 2024.

[14] J. Liu, X. Hou, W. Liu, L. Chen, Y. Kishiyama, and T. Asai, "Unified non-orthogonal waveform (uNOW) based on DFT-s-OFDM enhancement for 5G evolution and 6G," in *Proc. IEEE 33rd Annu. Int. Symp. Pers., Indoor Mobile Radio Commun. (PIMRC)*, Sep. 2022, pp. 217–222.

[15] N. Wu, Y. Zhang, H. Li, T. Zhang, J. Liu, X. Hou, and W. Liu, "Variational inference-based iterative receiver for unified non-orthogonal waveform (uNOW)," *IEEE Trans. Veh. Technol.*, vol. 73, no. 2, pp. 2848–2853, Feb. 2024.

[16] I. Gaspar, L. Mendes, M. Matthé, N. Michailow, A. Festag, and G. Fettweis, "LTE-compatible 5G PHY based on generalized frequency division multiplexing," in *Proc. 11th Int. Symp. Wireless Commun. Syst. (ISWCS)*, Aug. 2014, pp. 209–213.

[17] F. Schaich, T. Wild, and Y. Chen, "Waveform contenders for 5G–Suitability for short packet and low latency transmissions," in *Proc. IEEE 79th Veh. Technol. Conf. (VTC Spring)*, May 2014, pp. 1–5.

[18] Y. Yang, S. Dang, M. Wen, S. Mumtaz, and M. Guizani, "Bayesian beamforming for mobile millimeter wave channel tracking in the presence of DOA uncertainty," *IEEE Trans. Commun.*, vol. 68, no. 12, pp. 7547–7562, Dec. 2020.

[19] B. Ji, Y. Han, P. Li, S. Mumtaz, K. Song, C. Li, D. Wang, and H. Wen, "Research on secure transmission performance of electric vehicles under Nakagami-*m* channel," *IEEE Trans. Intell. Transp. Syst.*, vol. 22, no. 3, pp. 1881–1891, Mar. 2021.

[20] R. N. Hasyim and E. Y. Hamid, "Carrier frequency offset estimation using cyclic prefix in GFDM systems for machine type communication application," in *Proc. 8th Int. Conf. Intell. Syst., Model. Simul. (ISMS)*, May 2018, pp. 126–130.

[21] Z. Na, M. Zhang, M. Xiong, J. Xia, X. Liu, and W. Lu, "Pseudo-noise sequence based synchronization for generalized frequency division multiplexing in 5G communication system," *IEEE Access*, vol. 6, pp. 14812–14819, 2018.
[22] I. S. Gaspar, L. L. Mendes, N. Michailow, and G. Fettweis, "A synchronization technique for generalized frequency division multiplexing," *EURASIP J. Adv. Signal Process.*, vol. 2014, no. 1, pp. 1–10, Dec. 2014.
[23] H. Shayanfar, H. Saeedi-Sourck, and A. Farhang, "Low-complexity search method for CFO estimation in GFDM," *Electron. Lett.*, vol. 55, no. 6, pp. 355–357, Mar. 2019.
[24] B. Farhang-Boroujeny and H. Moradi, "OFDM inspired waveforms for 5G," *IEEE Commun. Surveys Tuts.*, vol. 18, no. 4, pp. 2474–2492, 4th Quart., 2016.
[25] P.-S. Wang and D. W. Lin, "Maximum-likelihood blind synchronization for GFDM systems," *IEEE Signal Process. Lett.*, vol. 23, no. 6, pp. 790–794, Jun. 2016.
[26] Y. Liu, X. Zhu, E. G. Lim, Y. Jiang, and Y. Huang, "Robust semi-blind estimation of channel and CFO for GFDM systems," in *Proc. IEEE Int. Conf. Commun. (ICC)*, May 2019, pp. 1–7.
[27] Y.-Y. Wang, S.-J. Yang, and T.-C. Lin, "Efficient carrier frequency offset estimation algorithm for generalized frequency division multiplexing systems," *Signal Process.*, vol. 172, Jul. 2020, Art. no. 107540.
[28] C. Qing, W. Yu, B. Cai, J. Wang, and C. Huang, "ELM-based frame synchronization in burst-mode communication systems with nonlinear distortion," *IEEE Wireless Commun. Lett.*, vol. 9, no. 6, pp. 915–919, Jun. 2020.
[29] C. Qing, S. Tang, C. Rao, Q. Ye, J. Wang, and C. Huang, "Label design-based ELM network for timing synchronization in OFDM systems with nonlinear distortion," in *Proc. IEEE 94th Veh. Technol. Conf. (VTC-Fall)*, Sep. 2021, pp. 01–05.
[30] C. Qing, S. Tang, X. Cai, and J. Wang, "Lightweight 1-D CNN-based timing synchronization for OFDM systems with CIR uncertainty," *IEEE Wireless Commun. Lett.*, vol. 11, no. 11, pp. 2375–2379, Nov. 2022.
[31] S. Ehsanfar, M. Matthe, D. Zhang, and G. Fettweis, "Interference-free pilots insertion for MIMO-GFDM channel estimation," in *Proc. IEEE Wireless Commun. Netw. Conf. (WCNC)*, Mar. 2017, pp. 1–6.
[32] J. Jeong, Y. Park, S. Weon, J. Kim, S. Choi, and D. Hong, "Eigendecomposition-based GFDM for interference-free data transmission and pilot insertion for channel estimation," *IEEE Trans. Wireless Commun.*, vol. 17, no. 10, pp. 6931–6943, Oct. 2018.
[33] Z. Na, Z. Pan, M. Xiong, J. Xia, and W. Lu, "Soft decision control iterative channel estimation for the Internet of Things in 5G networks," *IEEE Internet Things J.*, vol. 6, no. 4, pp. 5990–5998, Aug. 2019.
[34] Z. Na, Z. Pan, M. Xiong, X. Liu, W. Lu, Y. Wang, and L. Fan, "Turbo receiver channel estimation for GFDM-based cognitive radio networks," *IEEE Access*, vol. 6, pp. 9926–9935, 2018.
[35] U. Vilaipornsawai and M. Jia, "Scattered-pilot channel estimation for GFDM," in *Proc. IEEE Wireless Commun. Netw. Conf. (WCNC)*, Apr. 2014, pp. 1053–1058.
[36] S. Ehsanfar, M. Chafii, and G. Fettweis, "Time-variant pilot- and CP-aided channel estimation for GFDM," in *Proc. IEEE Int. Conf. Commun. (ICC)*, May 2019, pp. 1–6.
[37] S. Ehsanfar, M. Matthe, D. Zhang, and G. Fettweis, "Theoretical analysis and CRLB evaluation for pilot-aided channel estimation in GFDM," in *Proc. IEEE Global Commun. Conf. (GLOBECOM)*, Dec. 2016, pp. 1–7.
[38] B. Lim and Y.-C. Ko, "SIR analysis of OFDM and GFDM waveforms with timing offset, CFO, and phase noise," *IEEE Trans. Wireless Commun.*, vol. 16, no. 10, pp. 6979–6990, Oct. 2017.
[39] W. Li and J. C. Preisig, "Estimation of rapidly time-varying sparse channels," *IEEE J. Ocean. Eng.*, vol. 32, no. 4, pp. 927–939, Oct. 2007.
[40] C. R. Berger, S. Zhou, J. C. Preisig, and P. Willett, "Sparse channel estimation for multicarrier underwater acoustic communication: From subspace methods to compressed sensing," *IEEE Trans. Signal Process.*, vol. 58, no. 3, pp. 1708–1721, Mar. 2010.
[41] Y. Zeng, W. Leon, Y.-C. Liang, and A. Leyman, "A new method for frequency offset and channel estimation in OFDM," in *Proc. IEEE Int. Conf. Commun.*, vol. 43, Jun. 2006, pp. 4606–4611.
[42] H. Nguyen-Le, T. Le-Ngoc, and C. C. Ko, "Joint channel estimation and synchronization with inter-carrier interference reduction for OFDM," in *Proc. IEEE Int. Conf. Commun.*, Jun. 2007, pp. 2841–2846.
[43] R. Mo, Y. Huat Chew, T. Thiang Tjhung, and C. Chung Ko, "An EM-based semiblind joint channel and frequency offset estimator for OFDM systems over frequency-selective fading channels," *IEEE Trans. Veh. Technol.*, vol. 57, no. 5, pp. 3275–3282, Sep. 2008.
[44] H. Nguyen-Le and T. Le-Ngoc, "Joint synchronization and channel estimation for OFDM transmissions over doubly selective channels," in *Proc. IEEE Int. Conf. Commun.*, Jun. 2009, pp. 1–5.
[45] H. Nguyen-Le and T. Le-Ngoc, "ML-based joint estimation of carrier frequency offset and doubly selective channels for OFDM transmissions," in *Proc. IEEE 69th Veh. Technol. Conf.*, Apr. 2009, pp. 1–5.
[46] H. Nguyen-Le, T. Le-Ngoc, and C. Chung Ko, "RLS-based joint estimation and tracking of channel response, sampling, and carrier frequency offsets for OFDM," *IEEE Trans. Broadcast.*, vol. 55, no. 1, pp. 84–94, Mar. 2009.
[47] H. Nguyen-Le and T. Le-Ngoc, "Pilot-aided joint CFO and doubly-selective channel estimation for OFDM transmissions," *IEEE Trans. Broadcast.*, vol. 56, no. 4, pp. 514–522, Dec. 2010.
[48] J.-H. Choi, B.-J. Lim, Y.-J. Kim, and Y.-C. Ko, "Effect of timing and frequency synchronization errors on GFDM systems," in *Proc. Int. Conf. Inf. Commun. Technol. Converg. (ICTC)*, Jeju, Jeju, South Korea, Oct. 2015, pp. 1322–1325.
[49] A.-L. Yongwiriyakul and W. Suwansantisuk, "Time and frequency synchronization of GFDM waveforms," *IEEE Access*, vol. 12, pp. 61359–61374, 2024.
[50] Y. Liu, X. Zhu, E. G. Lim, Y. Jiang, and Y. Huang, "Semi-blind joint multi-CFO and multi-channel estimation for GFDMA with arbitrary carrier assignment," in *Proc. IEEE Global Commun. Conf. (GLOBECOM)*, Dec. 2019, pp. 1–6.
[51] Y. Liu, X. Zhu, E. G. Lim, Y. Jiang, and Y. Huang, "A semi-blind multiuser SIMO GFDM system in the presence of CFOs and IQ imbalances," *IEEE Trans. Wireless Commun.*, vol. 21, no. 1, pp. 48–63, Jan. 2022.
[52] S. Colieri, M. Ergen, A. Puri, and B. A, "A study of channel estimation in OFDM systems," in *Proc. IEEE 56th Veh. Technol. Conf.*, vol. 2, Sep. 2002, pp. 894–898.
[53] M. Colombo, Á. Hernández, and J. Ureña, "Low-complexity joint time synchronization and channel estimation for OFDM-based PLC systems," *IEEE Access*, vol. 7, pp. 121446–121456, 2019.
[54] H. Cheng, Y. Xia, Y. Huang, L. Yang, and D. P. Mandic, "Joint channel estimation and Tx/Rx I/Q imbalance compensation for GFDM systems," *IEEE Trans. Wireless Commun.*, vol. 18, no. 2, pp. 1304–1317, Feb. 2019.

ABUBAKAR MAGAJI BELLO was born in Ajingi, Nigeria, in October 1982. He received the B.Eng. degree from Bayero University, Kano, Nigeria, in 2007, and the M.Sc. degree from Zirve University, Gaziantep, Türkiye, in 2014. He is currently pursuing the Ph.D. degree in electrical and computer engineering with the King Mongkut's University of Technology Thonburi (KMUTT), Thailand.

In May 2017, he participated in a seminar on telecommunication network planning and optimization for developing countries with Wuhan Research Institute of Posts and Telecommunications, China. He is a Lecturer II with the Aliko Dangote University of Science and Technology (ADUSTECH), Wudil, Nigeria. His research interests include wireless communication, GFDM, and synchronization. Notably, in September 2022, he contributed as a Reviewer for Asia–Pacific Signal and Information Processing Association Annual Summit and Conference (APSIPA ASC).

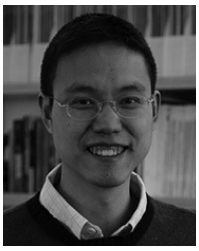

WATCHARAPAN SUWANSANTISUK (Senior Member, IEEE) was born in Uttaradit, Thailand, in December 1978. He received the B.S. degree in electrical and computer engineering and computer science from Carnegie Mellon University, Pennsylvania, in 2002, and the M.S. and Ph.D. degrees in electrical engineering from Massachusetts Institute of Technology, in 2004 and 2012, respectively.

He is currently an Assistant Professor with the King Mongkut's University of Technology Thonburi (KMUTT), Thailand. Before joining KMUTT, he spent summers with the University of Bologna, Italy, as a Visiting Research Scholar, and with Alcatel-Lucent Bell Labs, New Jersey, as a Research Intern. His research interests include wireless communications, synchronization, and statistical signal processing.

Dr. Suwansantisuk serves on the technical program committees for various international conferences and serves as the Symposium Co-Chair for the IEEE Global Communications Conference (2015). He received the Leonard G. Abraham Prize in the Field of Communications Systems from the IEEE Communications Society (2011), jointly with Professor Marco Chiani and Professor Moe Win; and the Best Paper Award from the IEEE RIVF International Conference on Computing and Communication Technologies (2016), jointly with Nasiroh Chedoloh.

IICKHO SONG (Fellow, IEEE) was born in Seoul, South Korea, in February 1960. He received the B.S.E. (magna cum laude) and M.S.E. degrees in electronics engineering from Seoul National University, Seoul, in 1982 and 1984, respectively, and the M.S.E. and Ph.D. degrees in electrical engineering from the University of Pennsylvania, Philadelphia, PA, USA, in 1985 and 1987, respectively.

He was a Member of the Technical Staff with Bell Communications Research, Morristown, NJ, USA, in 1987. In 1988, he joined the School of Electrical Engineering, Korea Advanced Institute of Science and Technology, Daejeon, South Korea, where he is currently a Professor. He has co-authored a few books, including *Advanced Theory of Signal Detection* (Springer, 2002), *Probability and Random Variables: Theory and Applications* (Springer, 2022), and *Fundamentals of Order and Rank Statistics* (Springer, 2024), and has published articles on signal processing and mobile communications.

Prof. Song is a fellow of Korean Academy of Science and Technology (KAST), Institution of Engineering and Technology (IET), and Korean Institute of Communications and Information Sciences (KICS); a Senior Member of the Institute of Electronics, Information, and Communication Engineers; and a member of the Acoustical Society of Korea (ASK), Institute of Electronics Engineers of Korea (IEEK), and Korea Institute of Information, Electronics, and Communication Technology. He received several awards, including the Young Scientists Award (KAST) in 2000, the Achievement Award (IET) in 2006, and the Hae Dong Information and Communications Academic Award (KICS) in 2006. He served as the Treasurer for the IEEE Korea Section; an Editor for the Journal of the ASK, Journal of the IEEK, the Journal of the KICS, and the *Journal of Communications and Networks* (JCN); and the Division Editor for JCN.

TAKUICHI HIRANO (Senior Member, IEEE) was born in Tokyo, Japan, in January 1976. He received the B.S. degree in electrical and information engineering from Nagoya Institute of Technology, Nagoya, Japan, in 1998, and the M.S. and D.E. degrees in electrical and information engineering from Tokyo Institute of Technology, Tokyo, in 2000 and 2008, respectively.

He was an Assistant Professor with Tokyo Institute of Technology, from 2002 to 2018. He is currently an Associate Professor with Tokyo City University, Tokyo. His research interests include electromagnetic theory, numerical analysis for EM problems, and antenna engineering.

Mr. Hirano was a recipient of the Young Engineer Award from the IEICE Japan in 2004, the IEEE AP-S Japan Chapter Young Engineer Award in 2004, and the IEEE MTT-S Japan Chapter Young Engineer Award in 2011.